Hydrodynamics of particle–wall interaction in colloidal probe experiments: comparison of vertical and lateral motion

2003 J. Phys.: Condens. Matter 15 3003

(http://iopscience.iop.org/0953-8984/15/19/304)

INSTITUTE OF PHYSICS PUBLISHING JOURNAL OF PHYSICS: CONDENSED MATTER

J. Phys.: Condens. Matter **15** (2003) 3003–3012 PII: S0953-8984(03)60509-6

Hydrodynamics of particle–wall interaction in colloidal probe experiments: comparison of vertical and lateral motion

Farida Benmouna[1] **and Diethelm Johannsmann**[2,3]

Max Planck Institute for Polymer Research, Ackermannweg 10, 55128 Mainz, Germany

E-mail: johannsmann@pc.tu-clausthal.de

Received 6 March 2003
Published 6 May 2003
Online at stacks.iop.org/JPhysCM/15/3003

Abstract

The hydrodynamic interaction between a colloidal particle attached to the tip of an atomic force microscope (AFM) and a wall has been investigated as a function of the angle of inclination of the cantilever with respect to the surface. For high inclination of the cantilever, the motion mostly occurs in the tangential direction. A frequency-dependent drag coefficient is extracted from the cantilever's Brownian motion. In agreement with theoretical predictions, the wall-induced drag for tangential motion is much weaker than that for vertical motion. Mechanical properties of the surface are more easily probed with tangential motion because the hydrodynamic effects do not mask the surface's intrinsic properties as much as for vertical motion.

1. Introduction

The hydrodynamic interaction between a particle and a wall is of much practical importance in colloidal flow [1, 2]. The pressure drop experienced by a granular material passing through a small tube or an orifice is to a significant extent given by the friction between the particles and the wall. While 'wall slip' is the exception rather than the rule in the flow of low-molecular-weight liquids [3], it is much more common for polymer melts or structured liquids such as polymer dispersions [4]. Plug flow, where most of the shear strain is located right at the wall, is a well-known phenomenon for complex fluids such as toothpaste and mayonnaise [5]. Even considering a simple colloidal dispersion of hard spheres, the bulk can undergo a 'jamming transition' in situations where the spheres located close to a flat surface still move easily [6].

[1] On leave from: Macromolecular Research Laboratory, Faculty of Sciences, University Aboubakr Belkaid, Tlemcen BP 119, Algeria.

[2] Present address: Institute of Physical Chemistry, Arnold-Sommerfeld-Street 4, 38678 Clausthal-Zellerfeld, Germany.

[3] Author to whom any correspondence should be addressed.

0953-8984/03/193003+10$30.00

Using colloidal spheres attached to an AFM tip [7], one can investigate such interactions between a colloidal sphere and a wall on the single-particle level. The motion of the tip is detected with very good sensitivity via the cantilever deflection. The sphere can be placed at an arbitrary distance from the wall or even be pushed against a soft surface with a constant vertical force. One drawback of the technique is that the cantilever—being larger than the sphere itself—affects the hydrodynamic interaction, as well. However, these corrections should be of small importance when the gap between the sphere and the wall becomes much narrower than the cantilever dimensions.

If the cantilever is soft enough, the dynamic interaction can be inferred from a statistical analysis of the cantilever's Brownian motion [8]. The power spectral density of the cantilever's thermal noise is a resonance curve. An effective spring constant and a drag coefficient can be derived from the shape of the curve. In the presence of relaxation phenomena, the interaction parameters are frequency dependent; the frequency dependence can be explicitly extracted from the noise spectra.

For steady movements, the hydrodynamic interaction between a sphere and a wall is predicted in detail by theory. For vertical motion, Reynolds stated in the late 19th century [9] that in the limit of a small gap width, D, the drag coefficient $\xi = F/v$ (F the force and v the speed) scales as the inverse distance, D^{-1}. More specifically, one has $\xi(D) \approx \xi_\infty R/D$ with R the particle radius and ξ_∞ the drag coefficient at infinity. Brenner later generalized this result to arbitrary distances. For tangential motion, a different scaling law applies: under the lubrication approximation ($D \ll R$) one has $\xi(D) \approx \xi_\infty (8/15) \ln(R/D)$ [10, 11]. The increase of the drag force with decreasing particle–wall distance is much weaker than for vertical motion.

In a recent paper we reported on the hydrodynamic interaction between a sphere and a wall, where the direction of motion was always close to vertical [12]. The predictions of Brenner were well obeyed with a small deviation at small distances. There is a slight frequency dependence of the drag coefficient $\xi(\omega)$, which also depends on the particle–wall distance. Here, we expand on these investigations, varying the direction of motion of the sphere by varying the angle between the surface and the cantilever.

2. Experiment and data analysis

A detailed description of the experimental set-up and procedure has been given in [8]. Figure 1 shows a sketch. A slight modification in the sample holder allows placement the sample at an arbitrary angle with respect to the cantilever. The sample was moved vertically and horizontally with a piezoelectric stage (P517.3CL, Physik Instrumente, Karlsruhe, Germany) equipped with a feedback control. We used V-shaped Si_3N_4 cantilevers (Digital Instruments) with a length $L = 100\,\mu$m. The angle between the direction of the cantilever's displacement and the surface is denoted as α. It is close to 75° when the surface is horizontal ('vertical' motion), and close to 5° when the sample is in an upright position ('lateral' motion). Due to instrumental constraints, neither purely vertical nor purely lateral motion can be realized in experiment.

In order to achieve well-defined sphere–plate geometry in the contact zone, glass spheres of 10 μm radius were glued onto the end of these cantilevers as shown in figure 2. The cantilevers were mounted in a commercial AFM head (Topometrix), which was placed on a 3D piezoelectric stage. Far away from the surface, the root mean square (rms) displacement $\langle \delta z^2 \rangle^{1/2}$ is 2.5 Å, corresponding to a spring constant of about $\kappa \sim 0.06$ N m^{-1} according to the equipartition theorem $\langle \delta z^2 \rangle \approx k_B T/\kappa$. The spring constant extracted from a fit of resonance curves to the noise power spectra agrees with this value. In water, the resonance frequency of the cantilever–sphere system is 13.5 kHz with a bandwidth Δf_{HBFW} of 5 kHz. The Q-factor was not changed by the sphere. Only the fundamental resonance frequency was

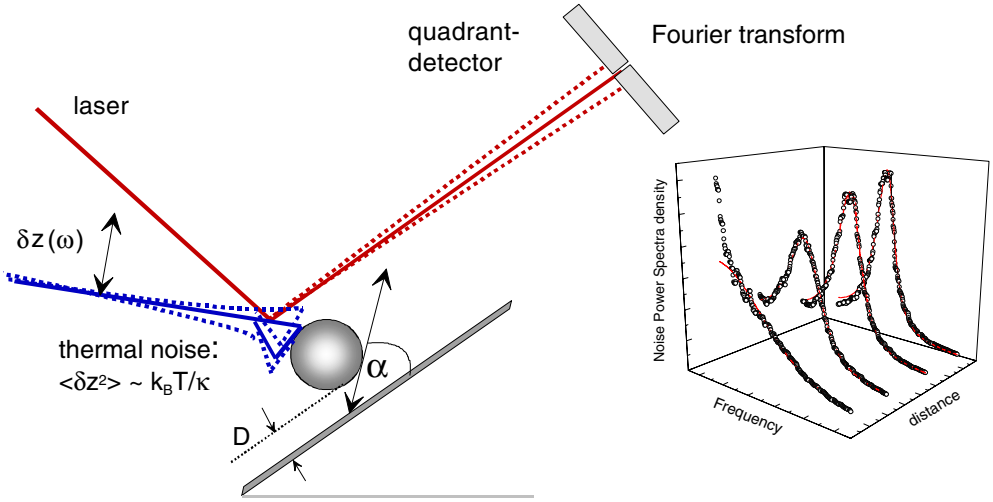

Figure 1. AFM noise analysis. The AFM cantilever with a sphere at its end mimics a colloidal particle near a wall. α is the angle between the direction of the cantilever deflection and the surface. The hydrodynamic effects strongly depend on α.

(This figure is in colour only in the electronic version)

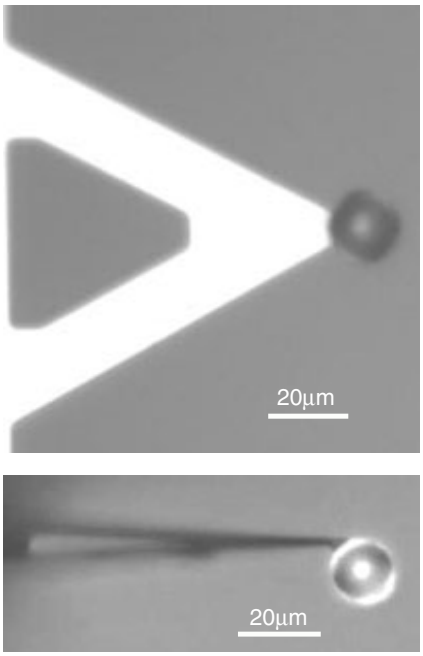

Figure 2. Optical micrographs showing the sphere glued onto the end of the cantilever. (a) Front view; (b) side view.

visible in the experimental frequency window of 1–100 kHz. While continuously approaching the sample, the noise was monitored with a Fourier analyser (HP 35670A) connected to the analogue output of the quadrant detector. The noise power spectra are on-line fitted with

resonance curves and converted to spectra of the drag coefficient $\xi'(\omega)$ [14]. A polymer cushion consisting of a 100 nm layer of spin-cast chitosan (Fluka) was used as a soft surface. At low pH (pH = 4 was used here) chitosan is charged and swells in water, forming a soft surface. The viscoelastic profiles obtained in vertical and lateral geometry are compared.

For soft surfaces, the definition of the origin of the distance scale, D, is somewhat ambiguous. Here, $D = 0$ is inferred from the difference between the force–distance curve and the line of constant compliance.

The noise power spectral density of the cantilever can be analysed to determine the viscoelastic properties of its environment, using the AFM tip as a local dynamic probe [13, 14]. According to the fluctuation dissipation theorem [15] the information contained in the thermal noise is equivalent to the outcome of force modulation spectroscopy [16]. In the simple-harmonic-oscillator approximation the power spectrum, $|\delta z(\omega)^2|$, is given by resonance curves of the Lorentz form [17, 18]:

$$|\delta z(\omega)^2| = 2k_B T \frac{\xi}{(\kappa - m\omega^2)^2 + \xi^2\omega^2} = 2k_B T \frac{\gamma}{m} \frac{1}{(\omega_0^2 - \omega^2)^2 + \gamma^2\omega^2} \tag{1}$$

with k_B the Boltzmann constant, T the temperature, κ the spring constant, m the mass, ω_0 the resonance frequency, and γ the width. These are 'effective' parameters in the sense that they reflect the cantilever's environment as well as its intrinsic properties. For instance, the spring constant increases when the cantilever interacts elastically with a substrate.

The simple-harmonic-oscillator approximation fails when the drag force depends on the speed at some past time. In this case the drag coefficient, ξ, becomes a complex function of frequency $\xi(\omega) = \xi'(\omega) + i\xi''(\omega)$, where the imaginary part ξ'' denotes an elastic (out-of-phase) component of the drag force. The real part of the drag coefficient is obtained as

$$\xi'(\omega) = \mathrm{Re}\left(\frac{2k_B T}{\omega^2\, \delta z^2[\omega]} \right) \tag{2}$$

where $\delta z^2[\omega]$ is the complex extension of the power spectral density [14].

3. Results and discussion

Figure 3 shows the power spectra $|\delta z^2(\omega)|$ ((a) and (c)) and the derived spectra of the drag coefficient $\xi'(\omega)$ ((b) and (d)) versus frequency for some selected distances. The substrate was a clean glass slide in MilliQ water. We compare data taken in the two limiting geometries which are $\alpha = 75°$ ('vertical' motion) and $\alpha = 5°$ ('lateral' motion). The continuous lines are fits to resonance curves (equation (1)).

The power spectral density strongly depends on whether the motion is vertical or tangential. For vertical motion, the resonance frequency shifts to the left on approach and the spectra become overdamped. Figures 3(b) and (d) show $\xi'(\omega)$ in double-logarithmic plots. The lines are fits to a power law $\xi' = \xi_{ref} \times (\omega/\omega_{ref})^{\beta}$. The power law was chosen as a fitting function on a purely heuristic basis. Data below 1 kHz were excluded from the fit because of contamination of the spectra by $1/f$ noise. The exponent β is termed the 'dispersion parameter'. The parameter β quantifies the deviation from the simple-harmonic-resonator model. It is negative in the presence of viscoelastic relaxation. Hydrodynamic interactions can also induce a non-zero exponent. A slightly positive exponent is found for large sphere–sample distances. However, as the sphere approaches the sample, β turns negative [12].

Figure 3(c) shows that the shape of the power spectra is affected by the surface much less when the sphere oscillates laterally. The peaks are sharper as compared to those of the vertical approach. The resonance frequencies even shift to higher values at small distances. The dispersion parameter (slope of fits in figure 3(d)) is positive for all data sets.

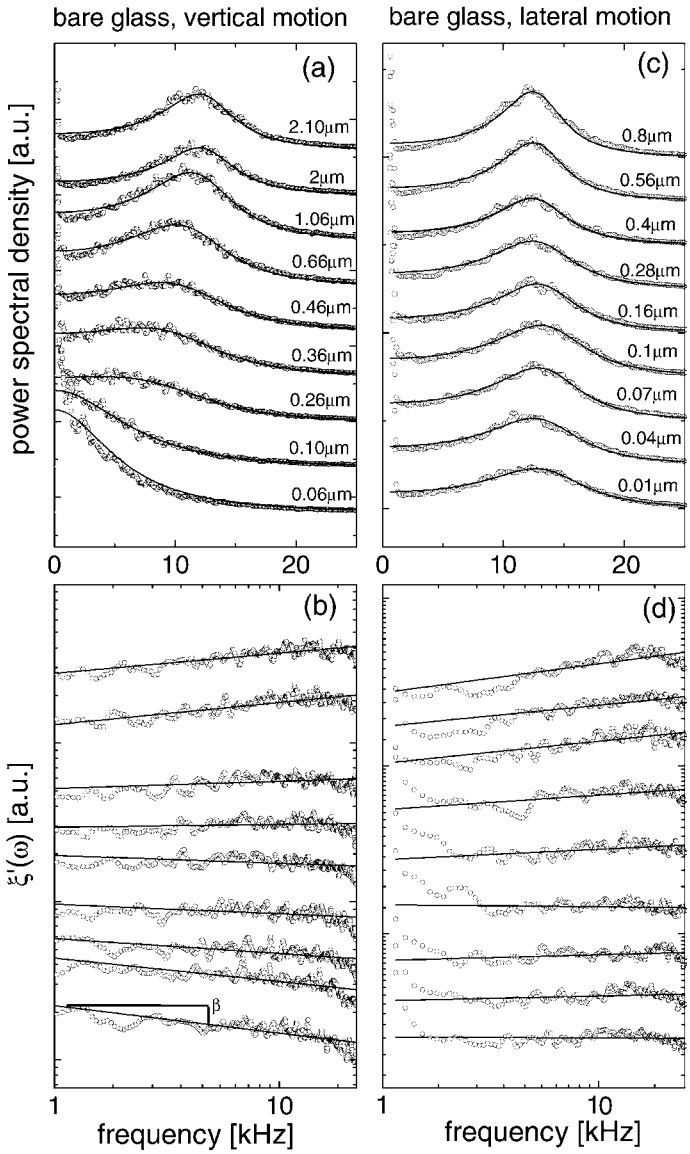

Figure 3. Noise power spectral densities ((a), (c)) and the real part of the frequency-dependent drag coefficient $\xi'(\omega)$ ((b), (d)). The substrate is bare glass placed in two different geometries. The solid curves in panels (a) and (c) are fits to the Lorentz function (equation (1)). When $\xi'(\omega)$ is plotted in double-logarithmic form, the slope corresponds to the power law exponent in a fit according to $\xi'(\omega) = \xi_{ref} \times (\omega/\omega_{ref})^{\beta}$. The curves are shifted vertically for clarity. The spectra in panels (b) and (d) correspond to the same distances as in panels (a) and (c).

Figure 4 shows the analogous results for the soft polymer cushion. For lateral motion, there is now some peak broadening, even though the spectra are not overdamped. The resonance frequency almost doubles as contact between the sphere and the polymer layer is made. The dispersion parameter turns negative when the sphere touches the surface. For vertical motion, on the other hand, the spectra are strongly overdamped.

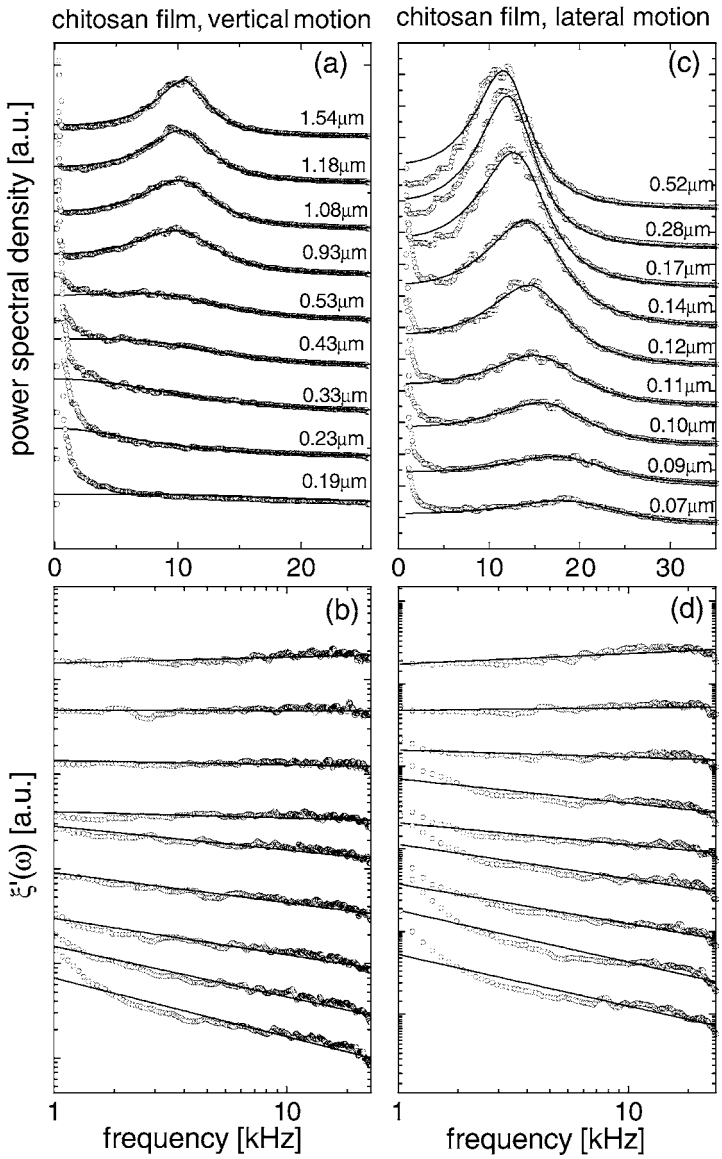

Figure 4. The same data as in figure 3, but where the substrate is a soft chitosan film.

In figure 5 some of the fit parameters from figures 3 and 4 are shown as a function of distance. These are the drag coefficient, $\xi(D)$ (panel (a)), the spring constant, $\kappa(D)$ (panel (b)), and the dispersion parameter, $\beta(D)$ (panel (c)). Naturally, the drag is found to be increased when comparing a soft to a hard surface in the same geometry. Note, however, that the curves for the tangential motion on the soft surface and for vertical motion on the hard surface cross. There is a distance range where the influence of the softness of the surface is more than outweighed by the influence of the geometry.

Panel (b) shows the spring constant κ, expressing an elastic interaction with the polymer-covered surface mediated by the polymer chains. κ increases at distances slightly above $D = 0$.

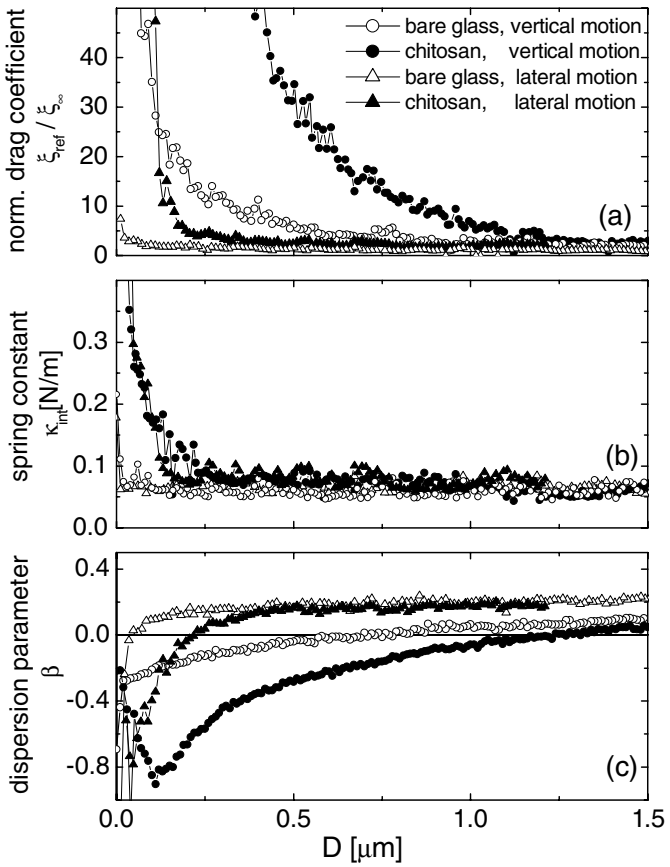

Figure 5. The drag coefficient at 10 kHz ξ_{ref} (a), spring constant κ (b), and dispersion parameter β (c) as a function of the normalized sphere–surface distance D/R. Hard and a soft surfaces are compared in the vertical and lateral position.

This has to do with the fact that $D = 0$ was defined via the line of constant compliance for the static force. The spring constant is more sensitive to weak interactions and therefore increases at a distance where the static force still is zero within the accuracy of the measurement. One could have chosen $D = 0$ as equal to the onset of the increase in spring constant, as well.

Panel (c) gives the dispersion parameter, β, quantifying the deviation from the simple-harmonic-oscillator model. The decrease of β with distance is much sharper for the lateral motion. Also, it occurs at smaller distances. For vertical motion and hard surfaces, β undergoes a sign reversal at $D/R \sim 0.07\,\mu$m. This sign reversal is one of the indications of hydrodynamic interaction. For lateral motion this sign reversal is shifted to a distance just barely above physical contact.

These experiments were repeated with bare glass, changing the inclination angle α in smaller steps. At intermediate angles, both normal and tangential components of the drag forces are present. Figure 6 displays the viscoelastic profiles for different angles. Panel (a) shows that the drag coefficient decreases smoothly when the surface is rotated from the horizontal position to the vertical position, while panel (c) indicates that β shifts upward.

Figure 7 shows the distance dependence of the drag coefficient in the two limiting geometries in more detail. The drag coefficient is normalized to its value at infinity and the distance D is normalized to R. The data are compared with the theoretical predictions

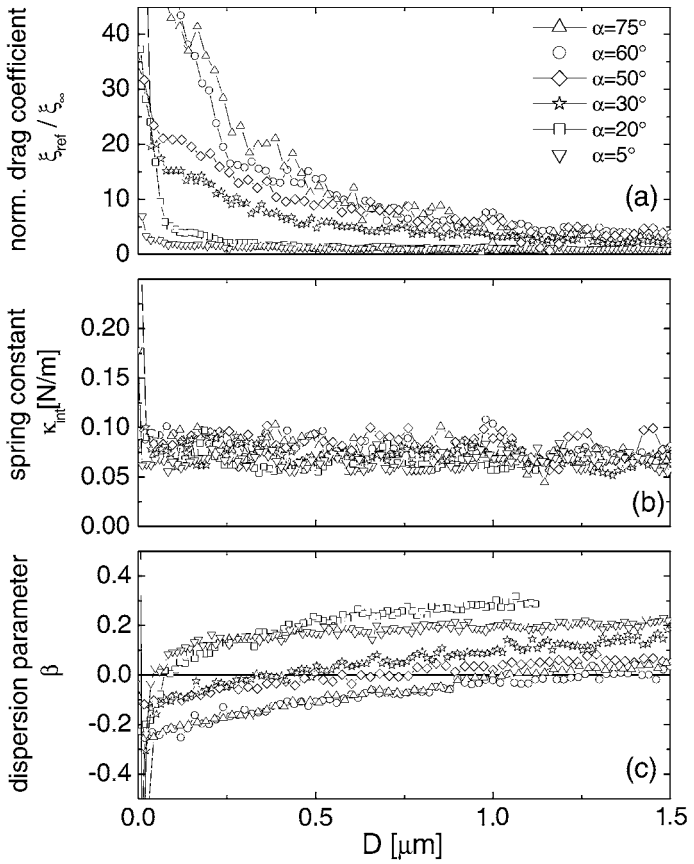

Figure 6. The same as figure 4, but for bare glass and several values of the angles α as indicated on the figure. Friction force increases as α increases from 5° (close to tangential) to 75° (close to vertical).

(grey continuous curves). The drag for the vertical motion agrees well with Brenner's equation

$$\frac{\xi}{\xi_\infty} = \frac{4}{3}\sinh(\alpha)\sum_{n=1}^{\infty}\frac{n(n+1)}{(2n-1)(2n+3)}\left[\frac{2\sinh((2n+1)\alpha)+(2n+1)\sinh(2\alpha)}{4\sinh^4((n+1/2)\alpha)-(2n+1)^2\sinh^2(2\alpha)}-1\right] \quad (3)$$

where $\alpha = \cosh^{-1}(D/R)$.

The solid black line is the prediction of Goldman *et al* for steady lateral motion [11]. There are no fit parameters. These authors predict a logarithmic dependence of the form

$$\frac{\xi}{\xi_\infty} = \frac{8}{15}\ln\frac{R}{D}. \quad (4)$$

The inset shows the data in logarithmic form. Clearly, the agreement is not quantitative. At this point we can only speculate about reasons for the disagreement. Note that equation (4) was derived for steady motion. For oscillatory motion, certain corrections may be necessary. Also the agreement might be better if the small vertical component ($\alpha \sim 5°$) could be removed.

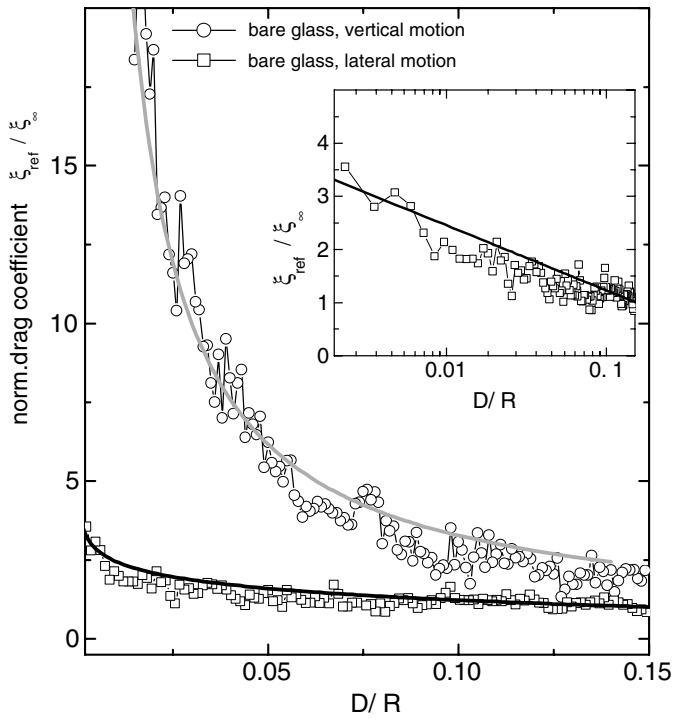

Figure 7. The normalized drag coefficient versus D/R for a bare glass for $\alpha = 5°$ and $75°$ as indicated in the figure. The black curve represents the lateral drag coefficient according to Goldman *et al* and the grey curve represents Brenner's prediction. The inset represents a semilogarithmic plot of the results for lateral motion.

4. Conclusions

The hydrodynamic interaction between a colloidal particle and a (soft) wall strongly depends on the direction of motion. For lateral motion the coupling is much weaker than for vertical motion. This is of importance not only for problems of flow of colloidal dispersions, but also for interfacial sensing. Many groups have recently used the AFM to probe dynamic forces in liquids [19, 20]. The forces do depend on the nature of the surface. Importantly, the effects of hydrodynamics (which may easily mask other forces of interest) are weaker for tangential motion than for vertical motion. A shearing motion is of much benefit, if the interest is in the surface itself, rather than the hydrodynamic interaction [21].

Acknowledgment

F Benmouna thanks the Alexander von Humboldt Foundation for financial support.

References

[1] Brenner H 1961 *Chem. Eng. Sci.* **16** 242
and see also
Happel J R and Brenner H 1983 *Low Reynolds Number Hydrodynamics* (Dordrecht: Kluwer) p 330
[2] Silbert L E, Landry J W and Grest G S 2003 *Phys. Fluids* **15** 1

[3] Vinogradova O I 1996 *Langmuir* **12** 5963
[4] Wang S Q 1999 *Adv. Polym. Sci.* **138** 227
[5] Larson R G 1999 *The Structure and Rheology of Complex Fluids* (Oxford: Oxford University Press)
[6] Wang S Q and Inn Y W 1995 *Polym. Int.* **37** 153
[7] Ducker W A, Senden T J and Pashley R M 1991 *Nature* **353** 239
[8] Roters A and Johannsmann D 1996 *J. Phys.: Condens. Matter* **8** 7561
[9] Reynolds O 1886 *Phil. Trans. R. Soc.* **177** 157
[10] Klein J and Kumacheva E 1998 *J. Chem. Phys.* **108** 6996
[11] Goldman A J, Cox R G and Brenner H 1967 *Chem. Eng. Sci.* **22** 637
[12] Benmouna F and Johannsmann D 2002 *Eur. Phys. J.* E **9** 435
[13] Roters A, Gelbert M, Schimmel M, Rühe J and Johannsmann D 1997 *Phys. Rev.* E **56** 3256
[14] Gelbert M, Biesalski M, Rühe J and Johannsmann D 2000 *Langmuir* **16** 5774
[15] See, for example,
Kubo R, Toda M and Hashitsume H 1985 *Statistical Physics* vol 2 (Heidelberg: Springer)
[16] Radmacher M, Tillmann R W and Gaub H E 1990 *Science* **268** 257
[17] Sader J E 1998 *J. Appl. Phys.* **84** 1
[18] Schaffer T E, Cleveland J P, Ohnesorge F, Walters D A and Hansma P K 1996 *J. Appl. Phys.* **80** 3622
[19] Maeda N and Senden T J 2000 *Langmuir* **16** 9282
[20] Bonaccurso E, Kappl M and Butt H J 2002 *Phys. Rev. Lett.* **88** 076103
[21] Ge S, Zhang Y, Pu W, Rafailovich M, Sokolov J, Buenviaje C, Buckmaster R and Overney R M 2000 *Phys. Rev. Lett.* **85** 2340